ORIGINAL PAPER

Geological structure and failure mechanism of an excavation-induced rockslide on the Tibetan Plateau, China

Lei Zhu[1] · Siming He[1,2,3] · Jihao Jian[1,3] · Jun Zhou[4] · Bin Liu[4]

Abstract

Rock slope failures are controlled by a complex interplay of geological structures and anthropogenic activities. In this study, data from structural geology, rock mass characterization, and ground-based monitoring networks are integrated into a numerical model. This model is used to explore the relationships among structural features, damages, anthropogenic activities, and slope failures occurring on the Tibetan Plateau in China. In particular, a model for the interpretation of brittle tectonic structures is illustrated, which characterizes the fracture patterns and explains the role of these features in the development of rock slope instability. Additionally, the relationships between tectonic structure-related fractures and slope failure mechanisms are investigated by characterizing the rock mass damage using the geological strength index. Finally, a numerical model is developed, which integrates the available data. It is found that the tectonic structure-related fractures controlled by an anticline are primarily responsible for slope failure, while an excavation was identified as its triggering mechanism. This research can serve as a reference for studies on excavation-induced rockslides.

Keywords Rockslide · Excavation · Failure mechanism · Tibetan Plateau

Introduction

Slope excavation for anthropogenic activities such as hydroelectric engineering and mining commonly induces slope failures. Excavations have triggered numerous recent landslide events (Peng et al. 2013; Troncone et al. 2014), resulting in large economic losses and casualties. Therefore, the assessment and prediction of slope failure mechanisms and stability during and after an excavation are crucial to reduce and prevent losses during these disasters (Najib et al. 2015; Kaya 2017).

The failure mechanism of excavation-induced rockslides depends on the structural features of the rock mass (e.g., spacing and persistence of joints) as well as on the geological features (e.g., lithology and topography), whereas structural patterns and rock mass damage are crucial factors in structure-controlled rockslides. Under complex geological conditions, the outcrops tectonic structures, including faults and shear zones, are frequently associated with rock mass (McSaveney et al. 1992; Fasani et al. 2004; Bois et al. 2012; Humair et al. 2013) and rock slope failures (Brideau et al. 2005, 2009; Hoek et al. 2005; Agliardi et al. 2009; Michel et al. 2009; Penna et al. 2016; Li et al. 2016; Cui et al. 2017). In general, the links between low rock mass quality (related to tectonic structures) and structurally controlled failure mechanisms are universal. Therefore, understanding how different slope failure mechanisms control rock fracturing can be significant in slope stability assessments.

A combination of field surveying, interpretation of monitoring data, and numerical simulations is used in this study to investigate an excavation-induced rockslide on the Tibetan Plateau, China. This was done to characterize the relation between certain tectonic structures and the occurrence of the rockslide. Furthermore, this study aims to evaluate the influence of tectonic structures and excavations on the slope

✉ Siming He
  hsm@imde.ac.cn

1   Key Laboratory of Mountain Hazards and Surface Process, Institute of Mountain Hazards and Environment, Chinese Academy of Sciences, Chengdu 610041, China

2   Center for Excellence in Tibetan Plateau Earth Sciences, Chinese Academy of Sciences, Beijing 100101, China

3   University of Chinese Academy of Sciences, Beijing 100049, China

4   China 19th Metallurgical Corporation, Chengdu 610031, China

movement and slope failure. For a better understanding of the kinematics of the slopes, monitoring networks based on a global positioning system are set up.

Geological setting

The study area is located in a tectonically active region on the eastern portion of the Tibetan Plateau, in the southeastern region of the Eastern Himalayan Syntaxis (Fig. 1a). The east–west trend of the tectonic structures gradually shifts north–south, crossing the Hengduan Mountains and forming a series of fluvial valleys (Wang et al. 2012; Yang et al. 2015), including the Jinsha River, Lanchang River, and Nu River valleys. Mesozoic rocks are widely distributed in this area, and they are primarily composed of Cretaceous, Jurassic, and Triassic stratified formations. The study area is located on the juncture of the Xizang, Sichuan, and Yunnan Provinces in the Hengduan Mountains, with a maximum elevation of 7556 m and an elevation difference up to 5000 m.

The regional geological structure is complex (Hou et al. 1993; Jin et al. 2002), as the study area has experienced numerous tectonic evolution stages, such as the Caledonian orogeny at the end of the early Paleozoic, plate deposition in the late Paleozoic, back-arc system formation from the Permian to the Early–Middle Triassic, development of a foreland basin from the Late Triassic to the Cretaceous, and finally the up-lift of the plateau in the Cenozoic. This has resulted in well-developed folds and faults (Fig. 2).

The study slope is located in the Changdu Basin, on a mountainside that lies between 4000 m a.s.l. at the ridge and 2900 m a.s.l. at the bottom, with an elevation difference of approximately 1100 m. It has a subtropical monsoon climate, with an average annual rainfall of 855.2 mm, mainly occurring from June to August.

More specifically, the slope is located in the middle of the Aitong fold, which is characterized by the development of a series of oblique–thrust faults. The faults strike northwest–southeast(F12, F13, and F14) and east–

Fig. 1 General settings of the study slope. **a** Location map of the study area. **b** Image of the study area
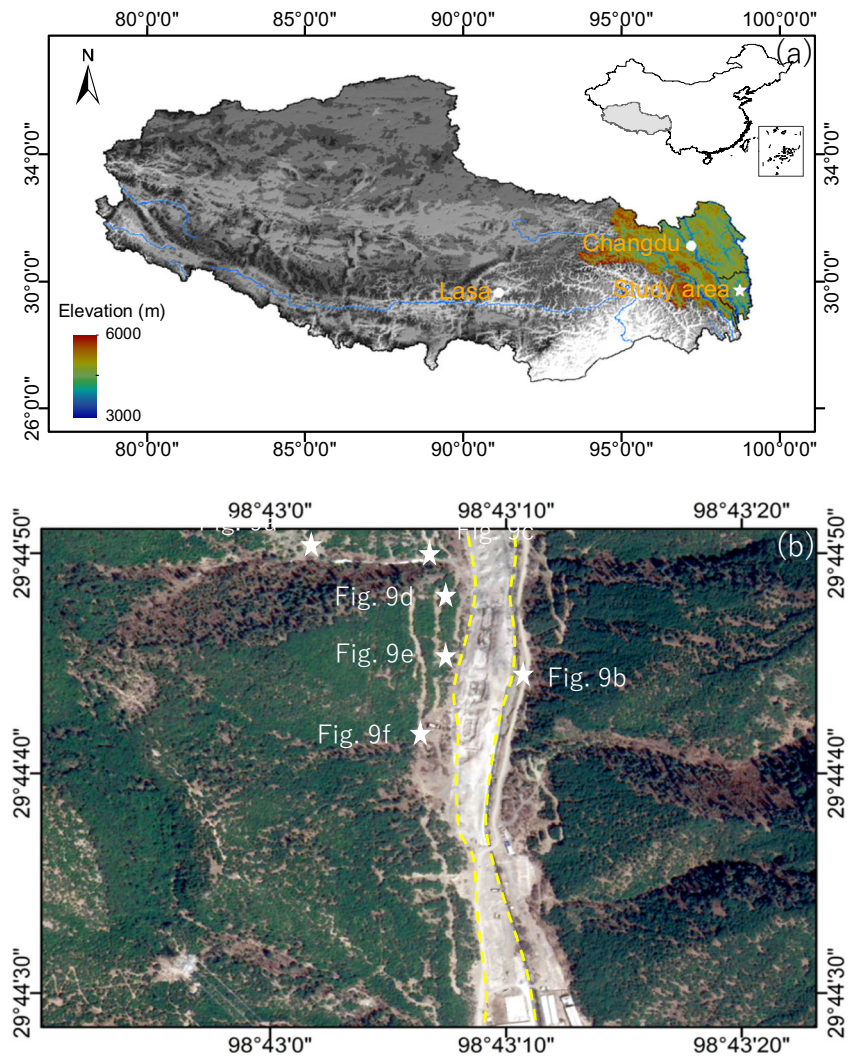
Fig. 2 Regional tectonic sketch map. (a) Tectonic sketch map of the SW, China; (b) regional tectonic map of the study area; and (c) profile along 1-1′ line
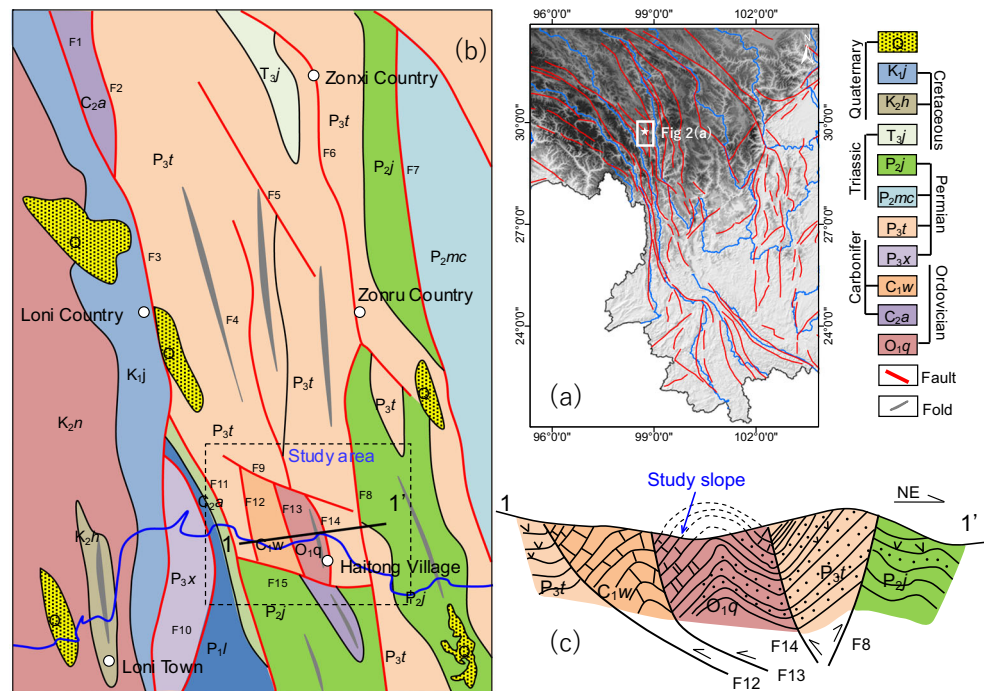
west (F9 and F15) (Fig. 2b). The fault plane of the northwest–southeast system strikes from N 15° E to N 50° E, with a dip of 45–60°.The east–west trending faults have a 60° dip. The Aitong anticline is located between faults F13 and F14.The exposed bedrock includes the upper Permian Tuoba Formation(P3t), Carboniferous Wuqingna Formation(C1w), lower Ordovician Qingnidon Formation(O1q), and middle Permian Jiaoga Formation(P2j). The layers that outcrop on the study slope belong to the lower Ordovician Qingnidon Formation(O1q) and consist of sandstone, limestone, and shale (Fig. 2c).
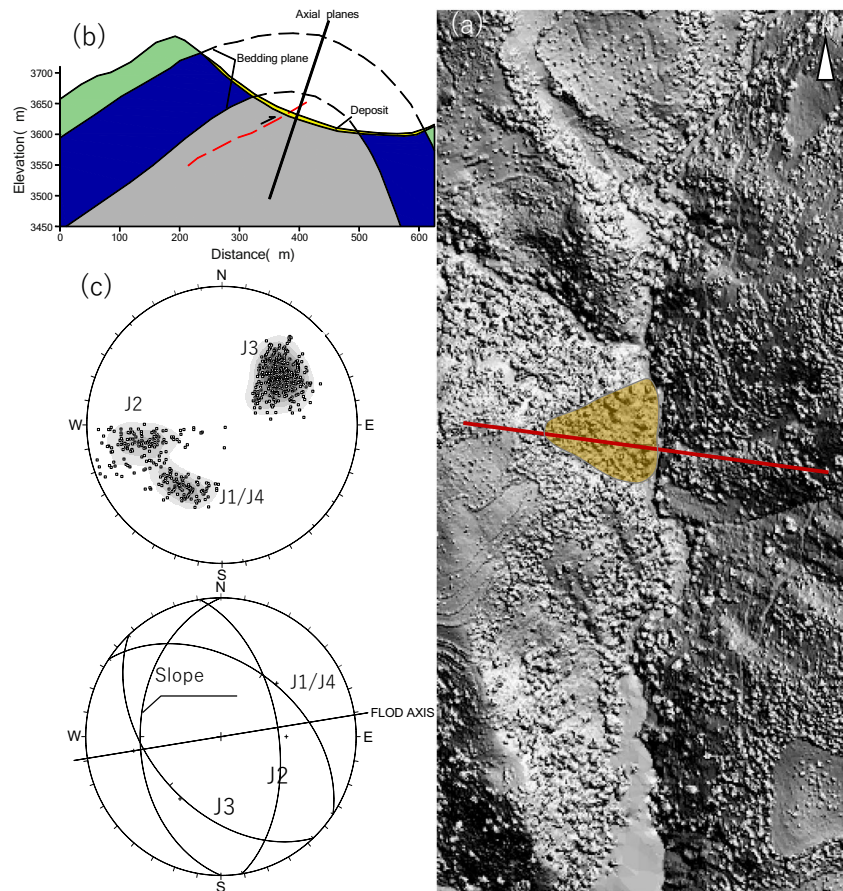
Fracturing

Fracturing sets

As reported by Reif et al. (2012) and Peacock et al. (2018), tectonic structures largely control the failure of an anticline slope, as the folding of the anticline can change the bedding and discontinuity set orientations. According to regional tectonics and field investigations, the study slope is located in an area characterized by the development of a series of northwest–southeast-striking faults. In particular, the northwest-striking Haitongou anticline was identified; it has a slope on the northwestern flank near the fold axis (Fig. 3a).

Four discontinuity sets, including the bedding plane, were identified based on the field investigations and tectonic features. The joint orientation was classified based on the

geometrical relationships with respect to the bedding plane and fold axis. The characteristics of the four discontinuity sets are as follows (Fig. 3c):

- J1—The dominant northwest-striking joint set (bedding plane) was found throughout the slope. Its orientation is sub-parallel to the slope direction with a dip angle of 40–50°, and it is characterized by dm-scale spacing and extremely high persistence (Fig. 4e).
- J2—The transverse joint set crosses the bedding planes perpendicularly (Fig. 4b). This set is present in nearly every domain and constitutes the primary fracturing pattern.
- J3 (J3a and J3b)—The densest joint set in the fold axis zone is sub- perpendicular to the bedding plane (J1). The kinematic indicators show that the J3 joint set systematically cuts the bedding plane. This set also cuts the J2 and J3b joint sets distributed in the northwestern and southeastern flanks of the anticline, forming a fan-like geometry with respect to the bedding plane (Fig. 4c and d).
- J4—This set is sub-parallel to the bedding plane (J1) on both flanks and sub-perpendicular to the joint set J3. It exhibits shear features, which are systematically filled with fragmented rock and mud. Most of joint set J4 developed along the bedding plane; thus, the length of the joint set exhibits good persistence. As a consequence, a decrease in the spacing along with an increase in the persistence of fracturing leads to a general reduction of the block size (Fig. 4e).

Fig. 3 (a) Hillshade map of Haitong anticline, showing the extension of the study area. (b) The cross sections highlight the fold geometry; (c) equal-angle, upper hemisphere stereo plots showing the main fracturing of the slope, J1 and J4: 200–220°/40–50°; J2: 280–300°/70–80°; J3: 40–50°/50–60°

Fracturing properties

Table 1 lists the properties of the joint sets. The transverse joint set (J3) is the most developed joint set in the study area. Its length ranges from centimeters to meters, and it exhibits

smaller spacing and restricted persistence compared with the other joint sets. Joint set J4 varies significantly across the slope, exhibiting a random distribution. In other words, the joints of this set are concentrated in certain areas, whereas they seldom occur in others. These joints are also closed and
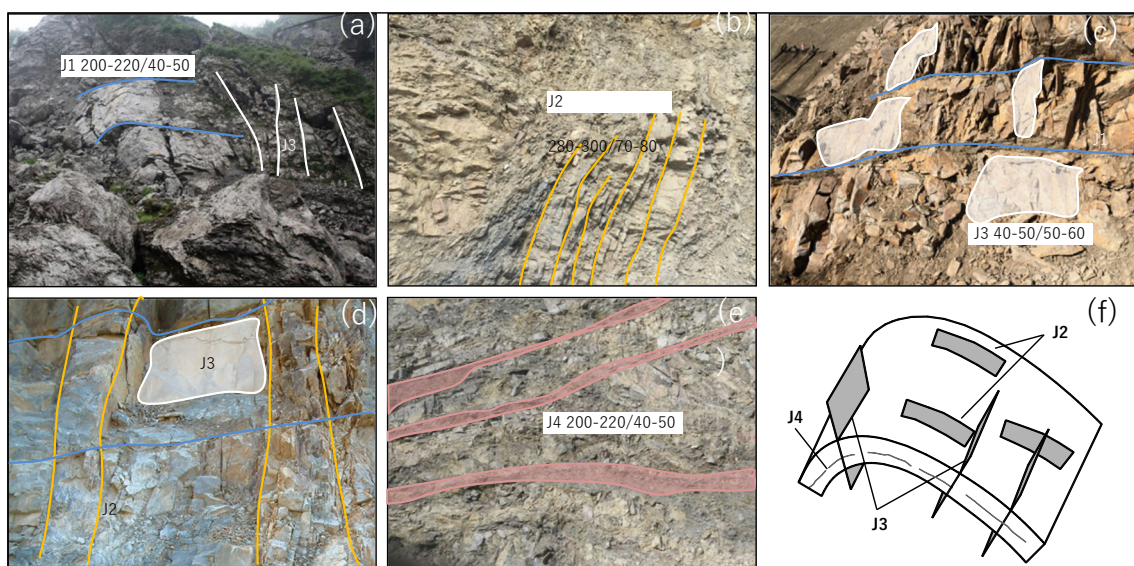

Fig. 4 (a)–(e) Field kinematic evidence of the joint sets. (f) Simplified representation of the major fracturing with respect to the bedding plane

Table 1 Characteristics of the discontinuity sets of the study slope

| Joint sets	Dir/dip	Density [n/m^2]	Persistence [m]	Aperture [cm]
J1	200–220/40–50	2–5	> 50	/
J2	280–300/70–80	0–5	0.2–0.5	0.5–1
J3	40–50/50–60	5–10	0.5–5	1–5
J4	200–220/40–50	0.5–1	> 50	/

Fig. 5 The schematic kinematic evolution of the fold and fractures, modified after Humair (2011), which represent four evolution stages of the anticline. (a) A pre-existing bedding planes. (b) The transverse joint sets among bedding planes began to form due to compression stress. (c) (d) The development of the dislocation zone along the bedding planes and form strike slip bedding faults
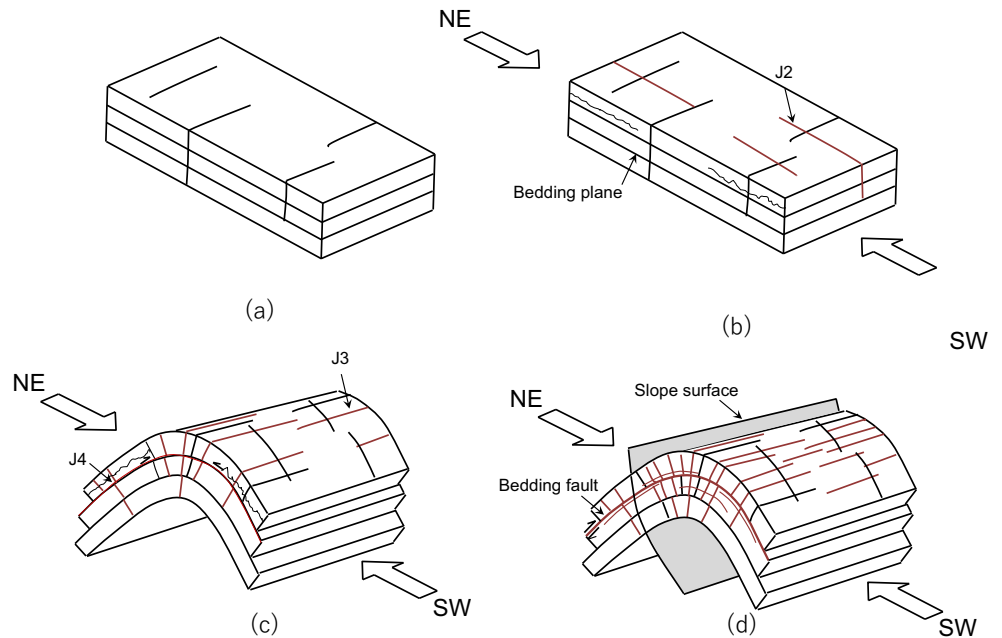
systematically mud-filled. In this regard, they differ from other joint sets, which are more variable.

The joint sets vary in thickness, orientation, and length, forming a complex system. The data from the field survey

Fig. 6 Conceptual structures model of study slope showing the tectonic influence on development of rock slope failure
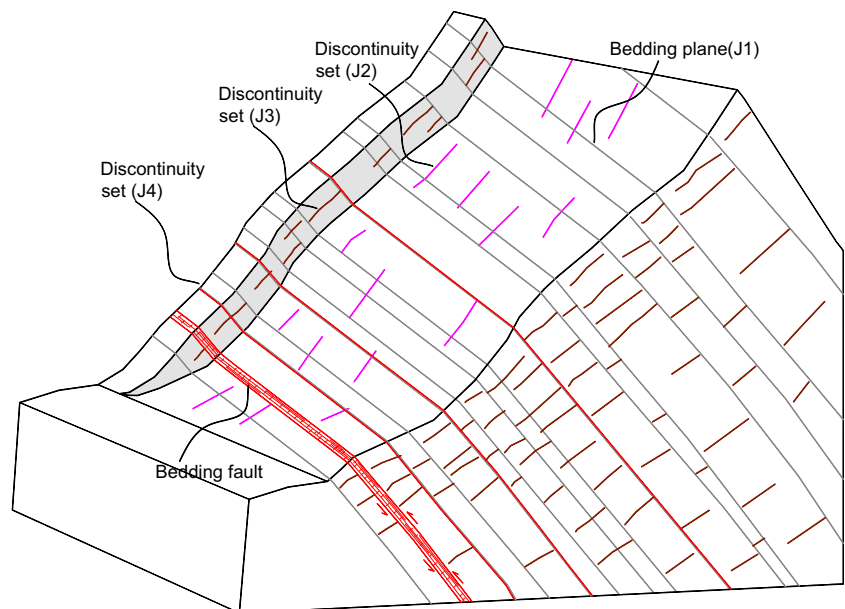
show that the density of the northwest-striking J3 joint is significantly higher than that of the other joints, whereas its length is shorter. In contrast, joint set J4 is longer but has the lowest joint density.

Fracturing pattern

Based on the field investigations and regional tectonics, the evolution of the anticline that contributed to the fracturing structures in the study slope was analyzed both in space and time. Considering the theoretical fold-related fracturing patterns and regional tectonic phases, an evolution model applicable to the fracturing pattern is proposed (Fig. 5).

Initially, when the strata planes were horizontal, a set of longitudinal joints formed in a direction parallel to the theoretical fold axis and perpendicular to the bedding planes (Fig.

5a). This can be interpreted as syn-sedimentary during subsequent progressive sediment compaction, as described by Price (1986). In the study area, the regional maximum principal stress had a northeast–southwest orientation in the early stage of the anticline formation. Tangential dislocations began to form among bedding planes because of the compressional stress. These joint sets also rotated during the folding of the strata (Fig. 6b). Engelder and Geiser (1980) and Bazalgette et al. (2010) previously documented the formation mechanisms of these joints.

The joint sets continued to grow (Fig. 5c), while the extensional joint set (J3) produced fan shapes with respect to the fold axis on both its sides. This can be interpreted as an indicator of stratum flexure. The transverse joint sets cogenetically developed in conjugate X-shaped sets and had a smaller dihedral angle. The development of the transverse

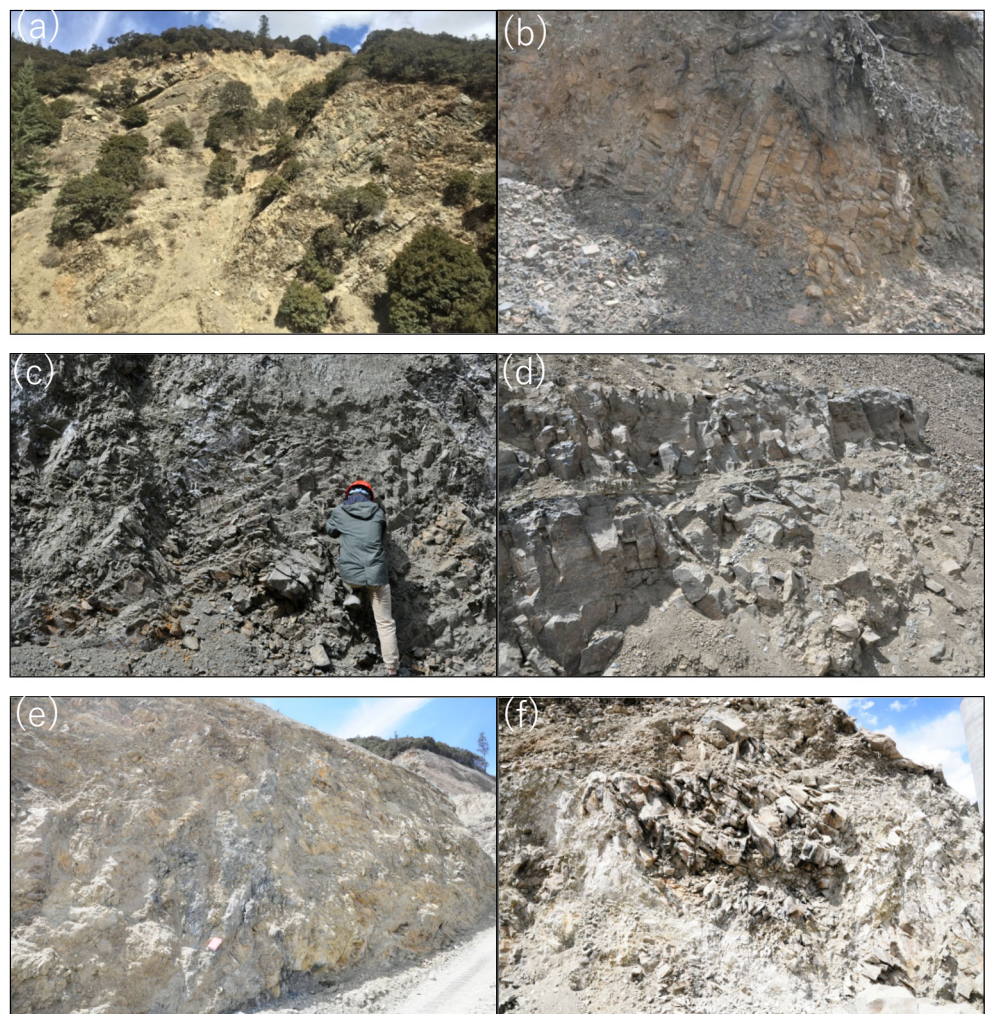**Fig. 7** Engineering geological map of the slope area
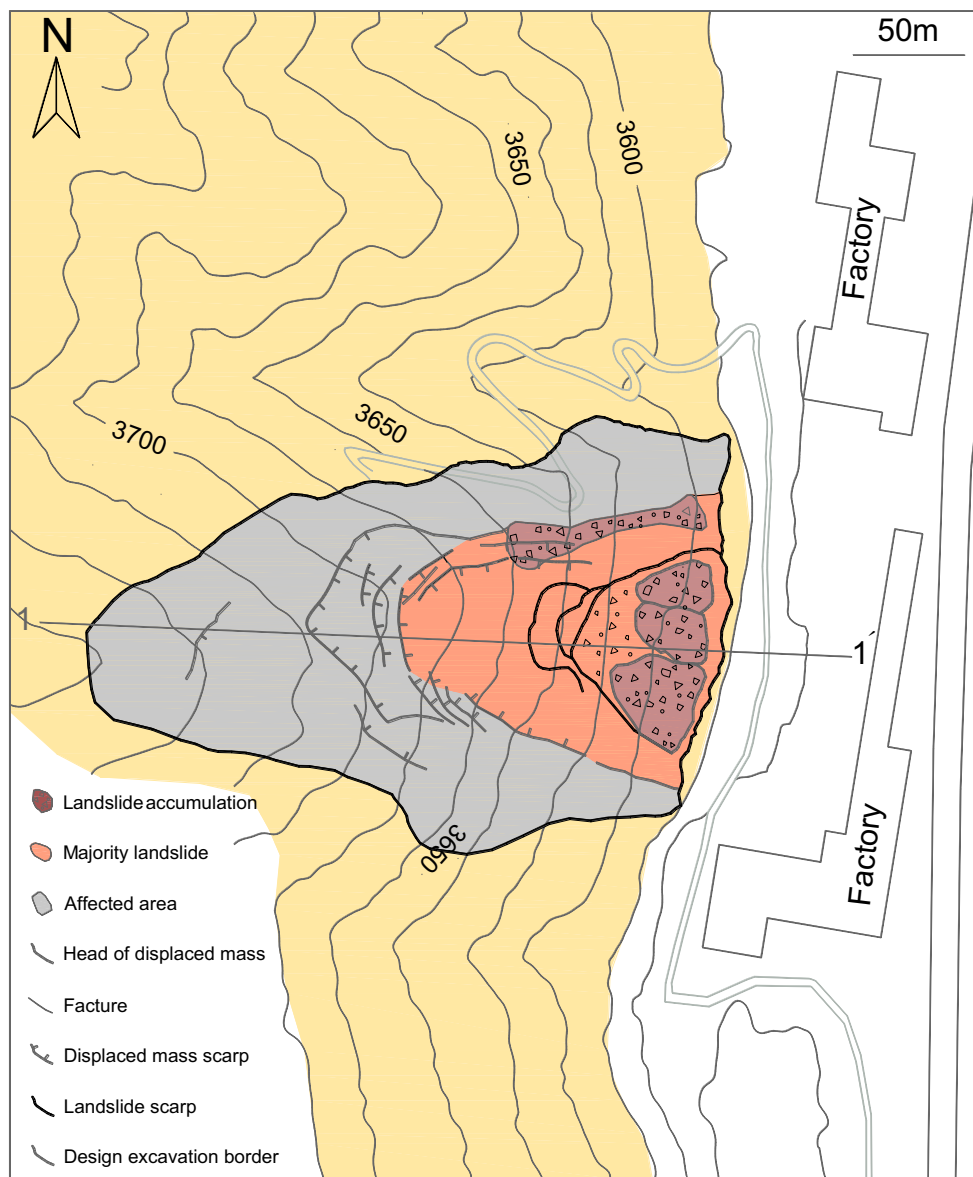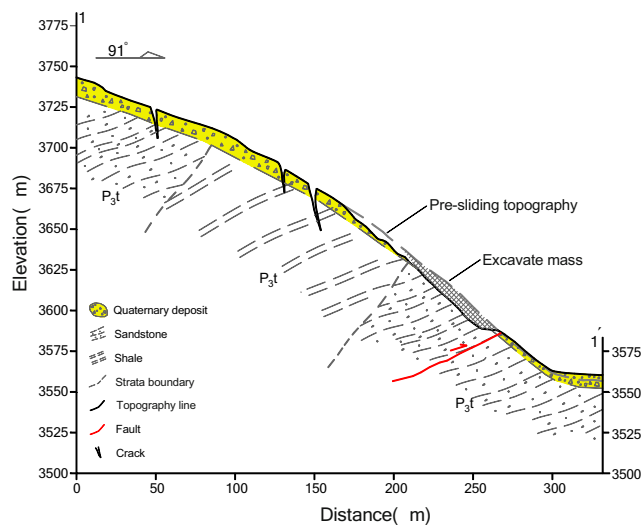
Fig. 8 Geological profile map of the slope, their position are shown in Fig. 8

joint sets contributed to rock fragmentation. Additionally, the development of the dislocation zone along the bedding planes

was rapid. The discontinuity set (J4) is thought to occur at this stage and is interpreted as an indicator of flexural slip folding.

With the folding of the anticline (Fig. 5d), the axial extension and discontinuity sets opened, especially in the fold axial zones. Small faults gradually formed because of the dislocations among the bedding planes. Moreover, the thrusting of inverse faults in the anticline increased the fragmentation of the rock slope. Figure 6 shows the conceptual structure model of the study slope.

Engineering geological characteristics

Slope structures

Field surveying and an engineering investigation of the rockslide are performed, which included exploratory boring and geophysical prospecting (Figs. 7 and 8). Thus, the geotechnical characteristics of the slope were identified. The rockslide affects a rock slope, for which the lithostratigraphy and rock structure were obtained via drill holes and site

Fig. 9 Typical geological structure of the slope area, their locations are shown in Fig. 1b, (**a**) the layered rockmass of the slope, (**b**) the layered rockmass in the opposite side of the valley, (**c**) (**d**) the dominant northwest-striking bedding plane, and (**e**)–(**f**) disintegrated rock

Fig. 10 (a) Rock structures of the rockslide in the drill holes, their locations are shown in (b), and (c) core of the drill holes

(a)

(b)

Quaternary deposit

Completely weathered

Highly weathered
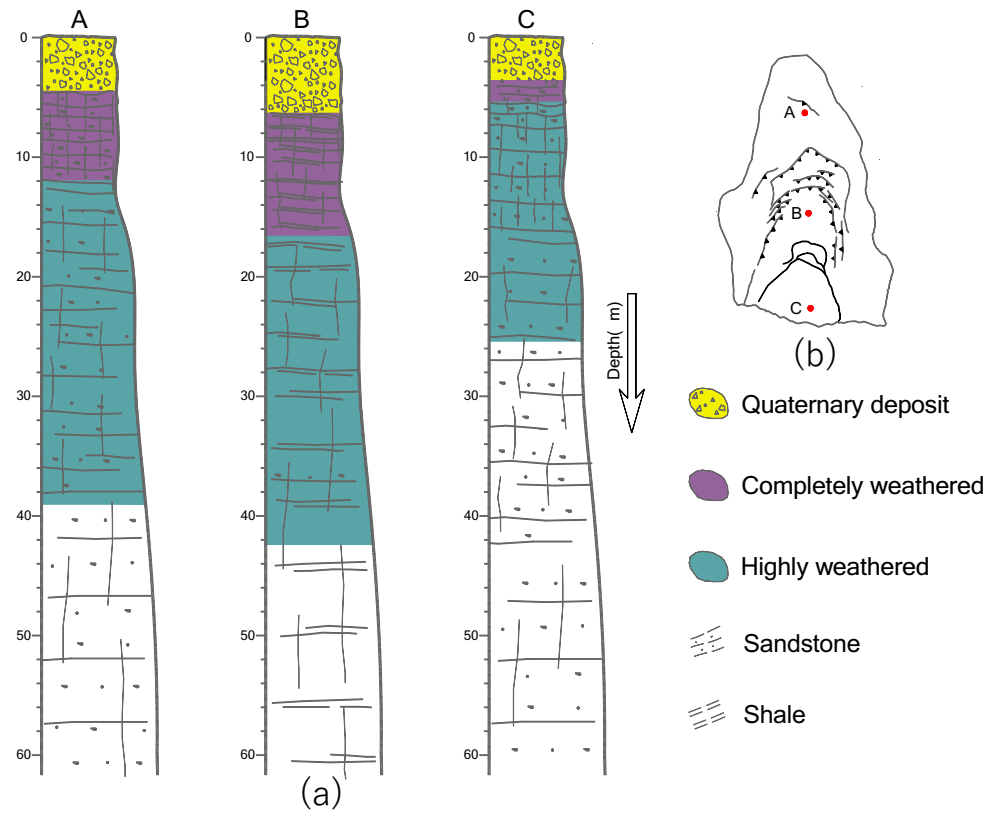
Sandstone

Shale

(c)

investigations (Figs. 9 and 10). The rock slope was found to comprise highly fractured rock masses, mainly composed of Ordovician sandstone intercalated with thin shale. The rock layer dips gently toward the inner side of the slope, with a strike of 200–220° and a dip angle of 40–50°. The joints are densely developed in the shallow portion of the rock, which can easily produce topple failures due to self-weight or because of the overburden from the overlying rock masses.

Table 2 Mechanics properties of the rock of the study slope

Properties	Fresh rock	Moderate weathered rock
Density (Kg/m^3)	2570	2400
Uniaxial compressive strength (MPa)	40	20
Cohesion (MPa)	2.1	1.4
Friction angle(°)	42	34

Three lithostratigraphic units were identified in the slope (Fig.10), which are described in detail as follows:

- Deposited soil—This unit is exposed at shallow depths on the slope and is composed of coarse-grained silt and strongly weathered rock fragments, which are widely distributed on the rockslide's surface, except on the lower part of the slope surface. The thickness of this unit ranges from 10 to 20 m, with a proportion of rock fragments from 20 to 40%.
- Disintegrated rock—This unit consists of severely crushed and highly fractured rock masses with numerous cracks. Certain cracks are filled with silty clay and are moderately to highly weathered, with sizes ranging from 0.2 to 0.4 m. The basic physical and mechanic parameters of the rock are listed in Table 2. The lithotypes of the highly fractured rock masses are sandstone and shale. The shale is mainly distributed in the central portion of the rockslide. The thickness of this unit ranges from 10 to 20 m.
- Blocky rock—The lithological composition of this rock mass is similar to that of the overlying units. The rock mass is lightly weathered and fractured, with fracture sizes ranging from a few centimeters to 1 m. The basic parameters of the rock are listed in Table 2. This unit is characterized by displaced rock blocks. The thickness of the highly weathered rock is undefined. The depth of the three drill holes in profile 1-1′(Fig. 10c) ranges between 25 and 42 m. At their maximum depth, the drill holes did not cross the fractured rock mass, indicating that the depth of the weathered rock is greater than 42 m.

Additionally, a geophysical investigation was performed to obtain seismic tomography profiles along the slope. These profile indicates that the depth of the fractured rock mass is 70–90 m. Figure 11 summarizes the seismic tomography data, and Table 2 lists the mechanic properties of the rock in the study slope.

Deformation characteristics

The failure of the study slope occurred after the excavation of the slope toe, at a location that was previously reinforced via soil anchors and sprayed concrete in April 2018. After the excavation, a number of concentrated tensile cracks along the rear section of the slope and longitudinal cracks on the shotcrete surface exposed the rear scarp and the lateral boundary of the rockslide, respectively (Fig. 12). During the site investigation, the tensile cracks were found to have strikes of 330–30°, and they were persistent with lengths of 5–20 m. Moreover, the crack walls exhibited a vertical displacement of 20–30 cm, with widths ranging from 10 to 50 cm. Extensive shear fractures were distributed along the lateral boundary of the slope. The direction of the shear cracks was parallel to the slope orientation, with orientations of 250–300°, dipping toward the inside of the lateral boundary. The thickness of the fractures ranged from 5 to 10 cm. Small cracks were also observed after the main rockslide event; however, no evident deformation or instability was visible in the affected zone.

Fig. 11 Seismic refraction tomography isovelocity contour lines of the slope
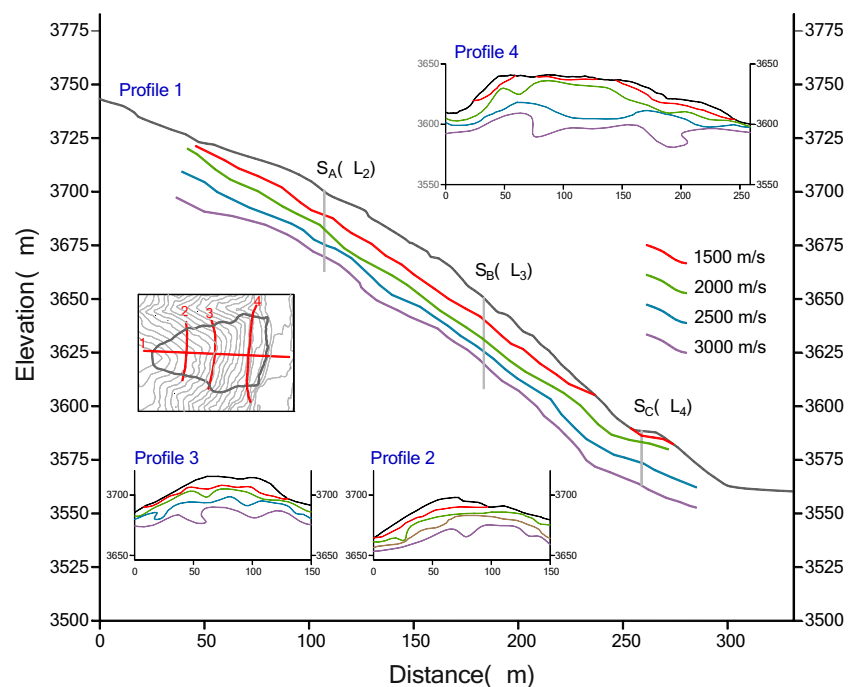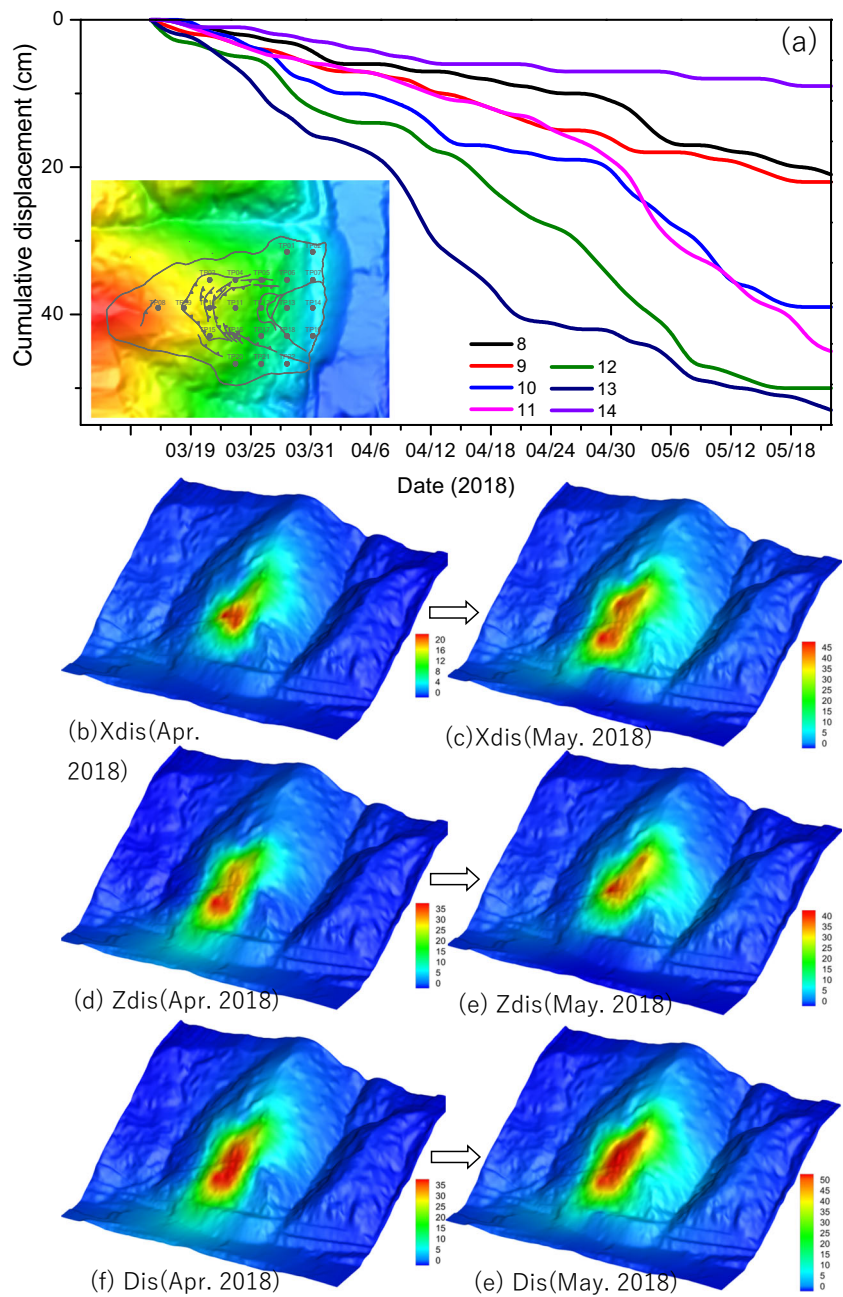
Fig. 12 Typical cracks of the study slope
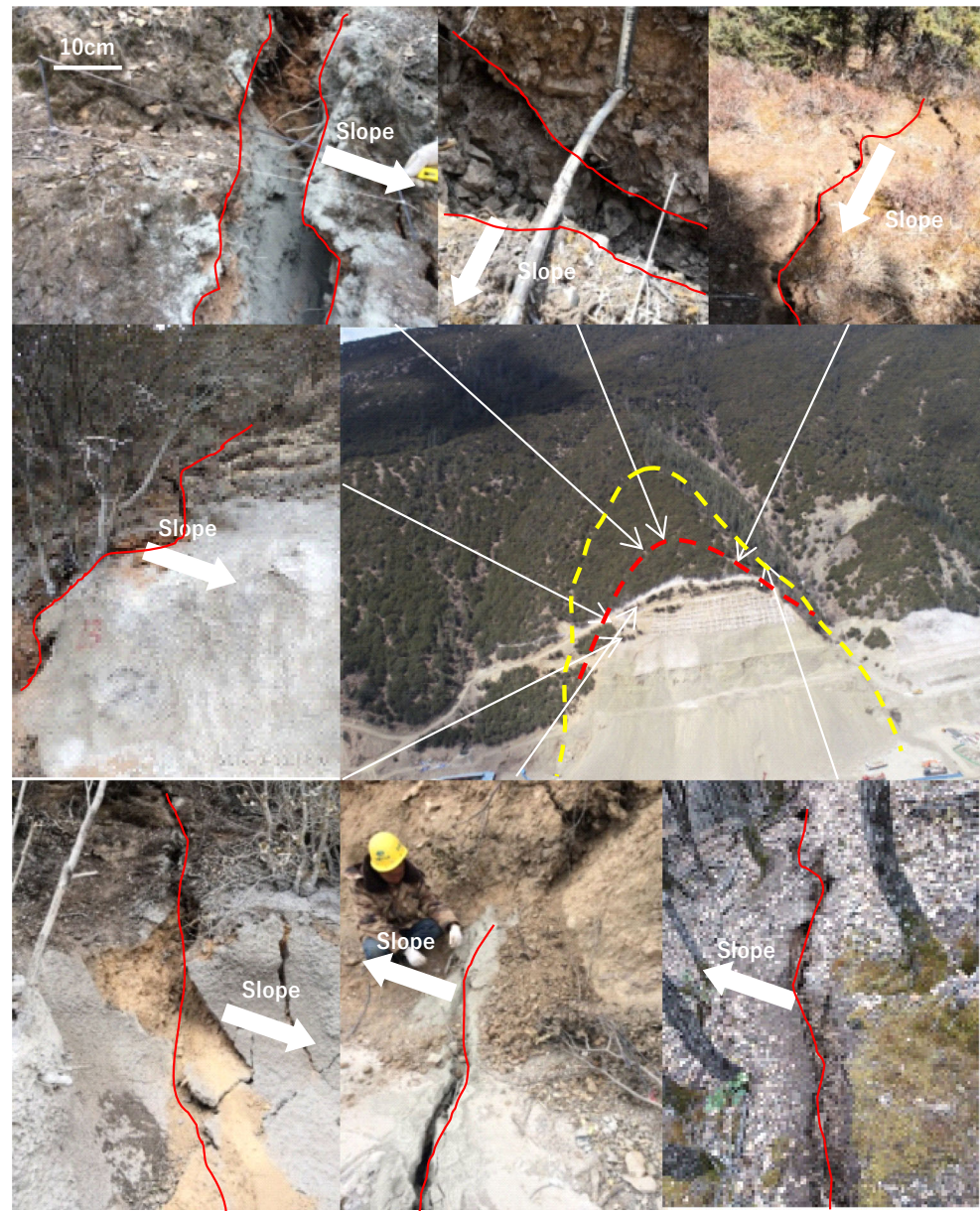
Monitoring analysis

A geotechnical monitoring network is installed on the slope before the excavation in March 2018, which included seven GPS surface displacement monitoring stations (Fig. 13a). After the excavation, 15 additional surface displacement monitoring stations were installed on the slope. The monitoring data were collected and analyzed to improve the understanding of the rockslide kinematics, mechanisms, and triggering factors. Figure 13a shows the ground surface displacement data from March to May 2018. Vertical and horizontal displacements were recorded during the excavation and reinforcement of the slope. The displacements gradually increased after the excavation, indicating that the latter significantly affected the slope deformation.

Throughout the monitoring period, the horizontal displacements were generally smaller than the vertical displacements during the early stage of the deformation process. The vertical displacements along profile 1-1′ (i.e., TP08, TP09, TP10, TP11, TP12, TP13, and TP14) were significantly smaller than the respective horizontal displacements. The vertical displacement zone was larger than the horizontal displacement zone, indicating that the deformation of the front section was greater than that of other areas. Horizontal displacements were dominant and generally larger than the 10-cm vertical displacements. The displacement rate remained generally stable throughout the monitoring period, except at monitoring points along the front section of the slope, indicating that the main rockslide body was in a creeping state.

Fig. 13 **a** Cumulative displacements measured by field monitoring. **b**–**g** The deformation evolution of the slope by fitting monitoring data

(b)Xdis(Apr. 2018)

(c)Xdis(May. 2018)

(d) Zdis(Apr. 2018)

(e) Zdis(May. 2018)

(f) Dis(Apr. 2018)

(e) Dis(May. 2018)

Failure mechanisms

According to the field investigations and drill holes, the slope rock mass structure can be divided into two main zones (Fig. 14). Geological strength index (GSI) values of 25–30 are characteristic of structurally controlled blocky rock masses, whereas lower GSI values (15–20) indicate disintegrated rock masses with a tendency to collapse (Fig. 15). Field evidence also suggests that the main rockslide occurred in a damaged rock zone characterized by GSI values of 15–20. As the damage is caused by rock fracturing, the disappearance of dominant fracture patterns, the block size,

and the mechanical properties makes the rock mass behave as one unit. Under suitable conditions, slope excavation can lead to slope failure along the boundary between the blocky and the disintegrated rock masses along a vertical profile.

Back analyses of the possible failure mechanisms and kinematics of the rockslide were conducted using the finite difference method (Flac 3D software). The analyses took both the pre-failure slope topography and the damaged rock mass into account. The rock mass properties were estimated via the Hoek–Brown approach (Hoek and Brown 1997; Marinos and Hoek 2000), whereas the GSI was used to estimate the rock mass damage scenarios. The material was characterized using

Fig. 14 Rock mass structures and the associated deformation zones, zone A is a concentrated deformation zone characterized by a lower GSI values, while zone B showing a small deformation
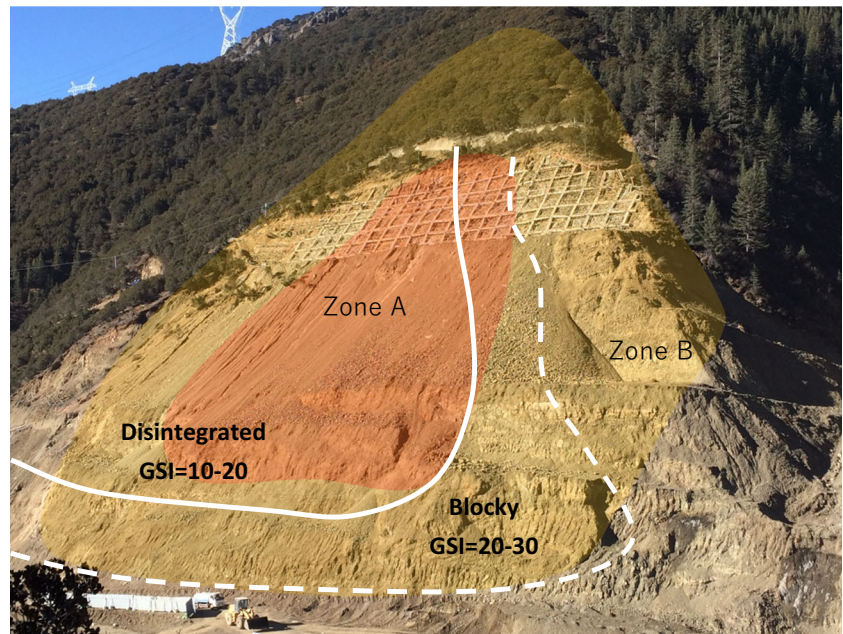
the Mohr–Coulomb failure criterion. The parameters used in the simulations of different rock mass damage scenarios corresponding to the GSI values of 15 and 25 are listed in Table. 3.

Model scenarios that incorporated the effects of the excavation were considered. The results of the simulations agreed with those of the monitoring and field investigations (in terms of deformation characteristics). In

Fig. 15 a Rock mass quality observed at the study rockslide based on the GSI. **b**–**d** Example of the different rock mass quality
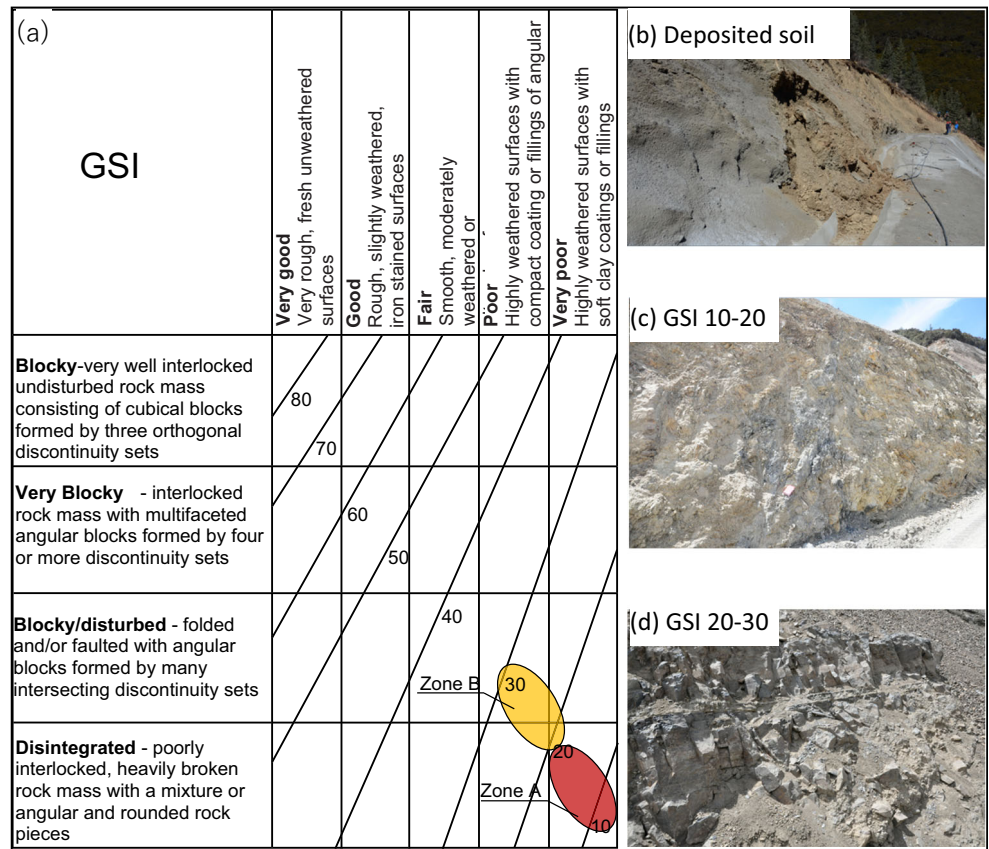
Table 3 Rock mass properties used in modeling corresponding to different rock mass damage scenarios

| Rock mass properties	Rock mass (GSI = 15)	Rock mass (GSI = 25)	Deposit soil
Density (Kg/m^3)	2200	2500	2000
Poisson's Ratio	0.28	0.25	0.30
Deformation modulus (GPa)	1.0	1.8	0.4
Tensile strength (MPa)	0.6	0.8	0.1
Cohesion (MPa)	0.8	1.2	0.4
Friction angle (°)	30	35	20

Fig. 16 Modeling results providing a picture of rockslide extent (**a**) and strain localization (**b**) match with the field and site investigation
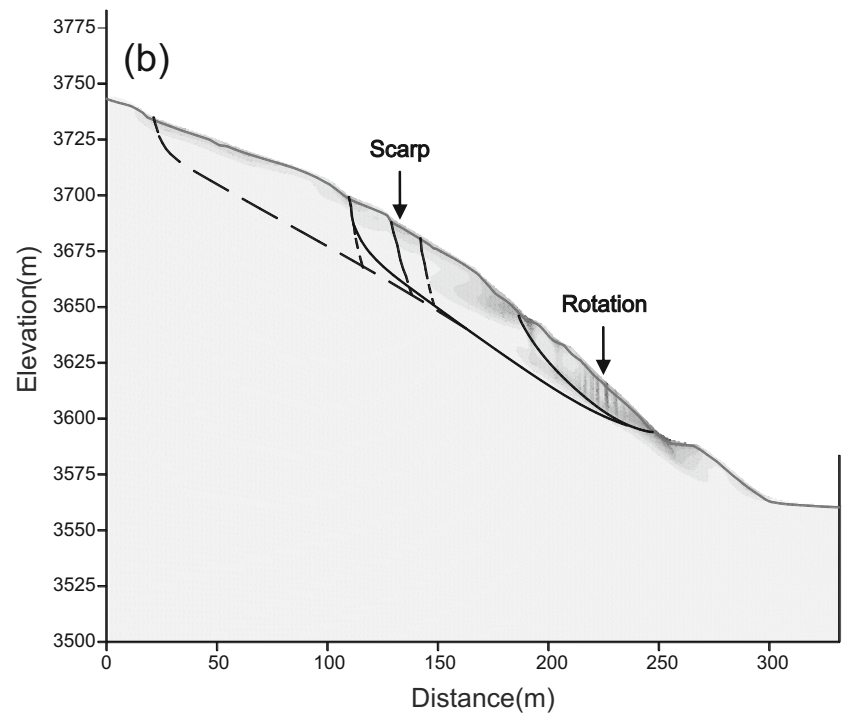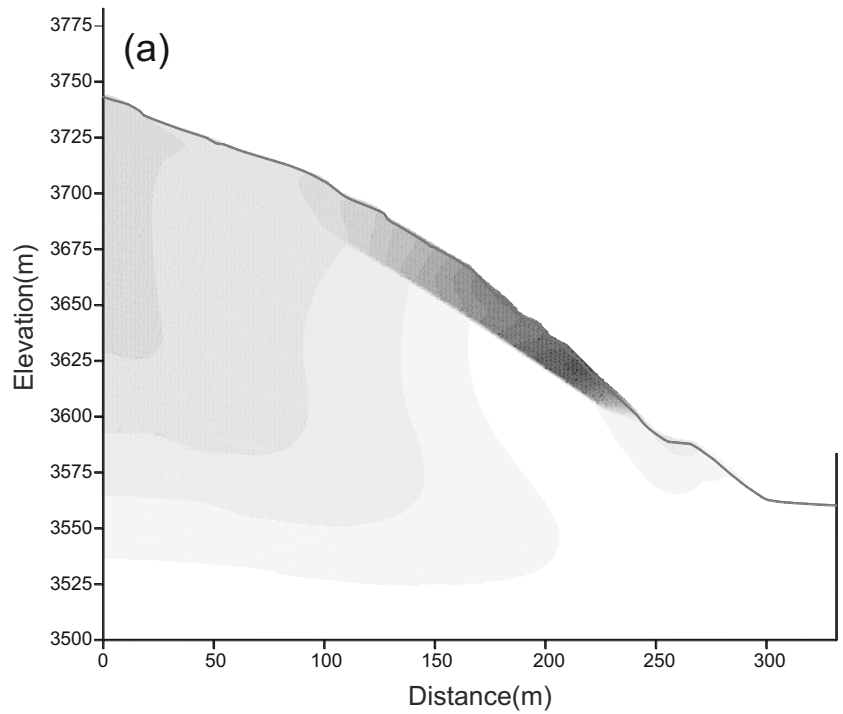
particular, the simulated displacements were compared with the monitoring data extracted from representative profiles. As shown in Fig. 16 and Fig. 17a, when the excavation is complete, a concentrated deformation zone appears along the lower section of the slope, indicating that the excavation-induced displacement zone propagated upwards. In addition, Fig. 16b shows that a shear zone developed along the interface between the disintegrated and blocky rock masses, corroborating the field observations. A sporadic shear zone developed along the rear section of the slope. The kinematic investigation performed through the monitoring network also reveals that a detachment zone developed within zone A of the rockslide (Fig. 17b); then, the failure propagates upward, resulting in deformation and cracks along the rear slope (Fig. 18).
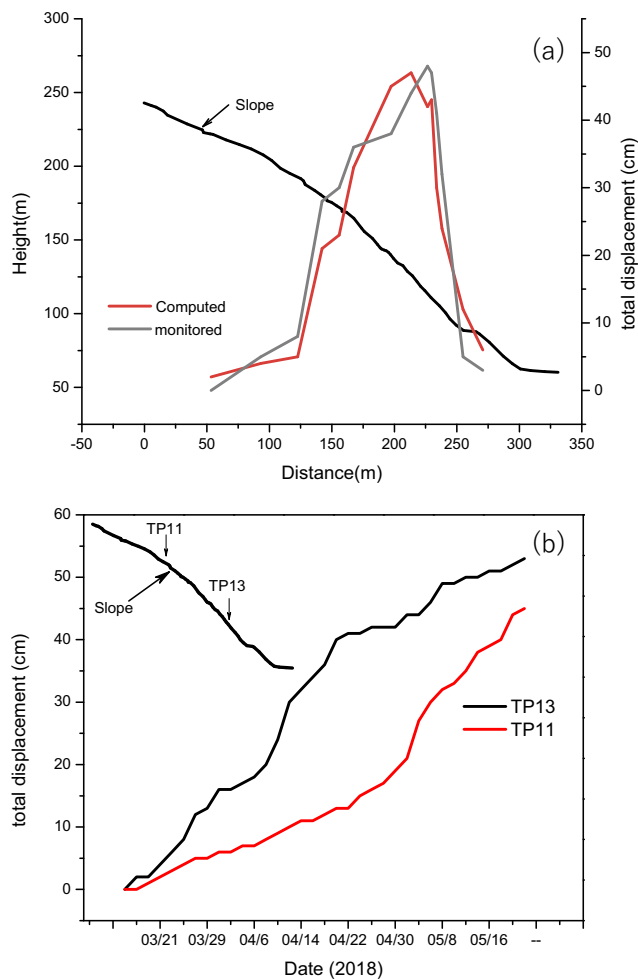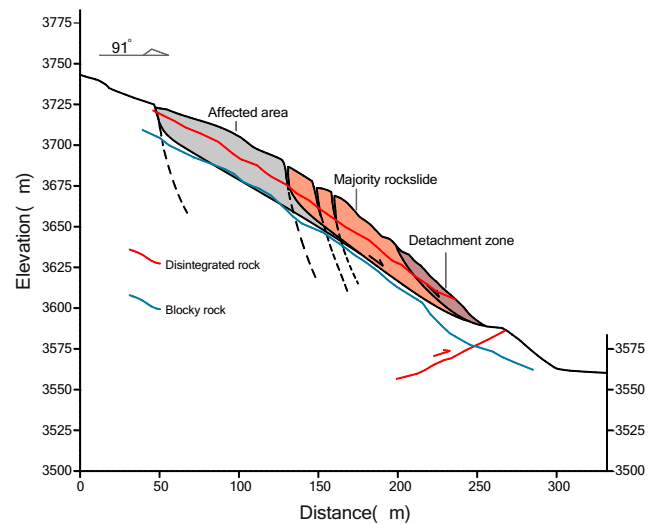
Fig. 18 Interpretative cross section of the rockslide, the sketches model also reveals that a detachment zone developed in the lower section of the slope, and then failure propagated upward, resulting in deformation and cracks along the rear slope, the result also suggests that the rock mass along the sliding surface was the boundary between the blocky and disintegrated rock mass

Conclusions

This study aimed to better understand the influence of tectonic folding on the development of a rock slope failure. Field investigations, geotechnical monitoring, and numerical modeling were used for structural interpretation and failure mechanism analysis. The main conclusions of the study are as follows.

The tectonic structure analysis highlighted the important role of the anticline during rock fracturing. Anticline folding controlled the tectonic structure-related fractures of the study slope. This conclusion is supported by the statistical analyses of the orientation of the joint sets and by a detailed classification of the geometrical relationships with respect to the bedding plane and fold axis. In particular, four discontinuity sets were identified: the dominant northwest-striking joint set (J1) that occurs throughout the slope, transverse joint set(J2) that is present in nearly every domain and represents the primary fracturing pattern, joint set (J3) that is distributed in the northwestern and southeastern flanks of the anticline, and shear joint set (J4) that developed along the bedding plane.

The rockslide occurred in a pre-damaged zone characterized by a disintegrated rock mass showing a definite correlation to the tectonic folding. The kinematic analysis performed using the data from the monitoring network revealed the development of a detachment zone within the central part of the rockslide, featuring a damaged rock mass characterized by GSI values of 15–20. The failure associated with this detachment was characterized by rotation or slumping. The displacements accelerated rapidly during the excavation from March

Fig. 17 a Comparison among profiles of simulated and monitored displacements. **b** Cumulative displacements of the points based on the monitoring network, TP11 is located in zone A, and TP13 is located in zone B, respectively

to May. Along with the concurrent development of tension cracks and secondary scarps, the activity of the deformation zone of the rockslide was likely enhanced by the excavation.

Finally, the analysis indicated that the rockslide on the study slope occurred in a pre-damaged rock mass. This pre-damage can be regarded as the factor responsible for slope failure, while the actual rockslide was triggered by the excavation.

References

Agliardi F, Zanchi A, Crosta GB (2009) Tectonic vs. gravitational morph structures in the central eastern alps (Italy): constraints on the recent evolution of the mountain range. Tectonophysics 474(1-2):0–270

Bazalgette L, Petit JP, Amrhar M, Ouana mi H (2010) Aspects and origins of fractured dip-domain boundaries in folded carbonate rocks. Struct Geol

Bois T, Stephane Bouissou, Jaboyedoff M (2012) Influence of structural heterogeneities and of large scale topography on imbricate gravitational rock slope failures: new insights from 3-d physical modeling and geomorphological analysis. Tectonophysics, 526–529(none), 147–156

Brideau MA, Stead D, Kinakin D, Fecova K (2005) Influence of tectonic structures on the hope slide, British Columbia, Canada. Eng Geol 80(3–4):242–259

Brideau MA, Yan M, Stead D (2009) The role of tectonic damage and brittle rock fracture in the development of large rock slope failures. Geomorphology 103(1):0–49

Cui S, Pei X, Huang R (2017) Effects of geological and tectonic characteristics on the earthquake-triggered Daguangbao landslide, China. Landslides

Engelder T, Geiser P (1980) On the use of regional joint sets as trajectories of paleostress fields during the development of the Appalachian Plateau, New York. J Geophys Res 85:319–341

Fasani GB, Esposito C, Maffei A, Mugnozza GS, Evans SG. (2004) Geological controls on initial failure mechanisms of rock avalanches in central Apennines (Italy). In: Larceda, E., Fontoura, Sayao (Eds.), Landslides: evaluation and stabilization. Balkema, Rotterdam, pp. 501–507. Rio de Janeiro

Hoek E, Brown ET (1997) Practical estimates of rock mass strength. Int J Rock Mech Min Sci Geomech Abstr 27(3):227–229

Hoek E, Marinos PG, Marinos VP (2005) Characterization and engineering properties of tectonically undisturbed but lithologically varied sedimentary rock masses. Int J Rock Mech Min Sci 42(2):277–285

Hou ZQ, Mo XX, Tan J, Hu S, Luo Z (1993) The eruption sequences of basalts in the Yidun island arc, Sanjiang region and evolution of rift to island arc. Acta Geosicientia Sinica 16(2):12–27

Humair F (2011) Turtle Mountain anticline (Alberta, Canada): rock slope stability related fracturing-folding, fracturing, rock mass condition, slope stability investigations geological modeling. (unpublished master thesis) Institute of Geomatics and Risks Analysis and Institute of Geology and Paleontology, University of Lausanne, Switzerland

Humair F, Pedrazzini A, Epard JL, Froese CR, Jaboyedoff M (2013) Structural characterization of turtle mountain anticline (Alberta, Canada) and impact on rock slope failure. Tectonophysics 605: 133–148

Jin XC, Wang DN, Liu Q (2002) Two cenozoic palynological assemblages of the Kurha section, Kuqa, Xinjiang and their age and environmental significance. Regional Geology of China 21(12):823–833

Kaya A (2017) Geotechnical assessment of a slope stability problem in the Citlakkale residential area (Giresun, NE Turkey). Bull Eng Geol Environ 76(3):875–889

Li X, Wu Y, He S, Su L (2016) Application of the material point method to simulate the post-failure runout processes of the Wangjiayan landslide. Eng Geol 212:1–9

Marinos P, Hoek E, (2000) GSI: a geologically friendly tool for rockmass strength estimation. Proceedings of the GeoEng2000 at the International Conference on Geotechnical and Geological Engineering, Melbourne. Technomic Publishers, Lancaster, pp. 1422–1446.s

McSaveney MJ, Chinn TJ, Hancox GT (1992) Mount Cook avalanche of 14 December1991, New Zealand. Landslide News August, pp 32–34

Michel J, Demers D, Locat J, Locat A, Turmel D (2009) Use of terrestrial laser scanning for the characterization of retrogressive landslides in sensitive clay and rotational landslides in river banks. Can Geotech J 46(12):1379–1390

Najib N, Fukuda D, Kodama J, Fujii K (2015) The deformation modes of rock slopes due to excavation in mountain-type mines. Mater Trans 56(8):1159–1168

Peacock DCP, Sanderson DJ, Rotevatn A (2018) Relationships between fractures. J Struct Geol 106:41–53

Peng M, Li XY, Li DQ, Jiang SH, Zhang LM (2013) Slope safety evaluation by integrating multi-source monitoring information. Struct Saf 49:65–74

Penna IM, Abellán Antonio, Humair F, Jaboyedoff M, Daicz S, & Fauqué Luis (2016) The role of tectonic deformation on rock avalanche occurrence in the Pampeanas ranges, Argentina, Geomorphology

Price RA (1986) The southeastern Canadian Cordillera: thrust faulting, tectonic wedging, and delimitation of the lithosphere. J Struct Geol 8:239–254

Reif D, Decker K, Grasemann B, Peresson H (2012) Fracture patterns in the Zagros fold-and-thrust belt, Kurdistan region of Iraq. Tectonophysics, 576–577

Troncone A, Conte E, Donato A (2014) Two and three-dimensional numerical analysis of the progressive failure that occurred in an excavation-induced landslide. Eng Geol 183:265–275

Wang XY, Lu HY, Vandenberghe J, Zheng S, Van BR (2012) Late Miocene uplift of the NE Tibetan Plateau inferred from basin filling, planation and fluvial terraces in the Huang Shui catchment. Glob Planet Chang 88:10–19

Yang R, Willett SD, Goren L (2015) In situ low-relief landscape formation as a result of river network disruption. Nature 520(7548):526–529